Experimental study of the reduction and removal of turn-on snubber for IGCT based MMC submodule using fast silicon diodes

Arthur Boutry[1], Cyril Buttay[2], Besar Asllani[1], Bruno Lefebvre[1], Eric Vagnon[2], Dong Dong[3]

[1] SuperGrid Institute
23 rue Cyprian
F-69100 Villeurbanne,
France

[2] Univ Lyon, Ecole Centrale de Lyon,
INSA Lyon, Université Claude Bernard Lyon 1,
CNRS, Ampère, UMR5005,
69130 Ecully, France

[3] Center for Power Electronics Systems
The Bradley Dept. of Electrical and Computer Eng.
Virginia Polytechnic Institute and State University
Blacksburg, VA 24061, USA

E-mail: arthur.boutry@supergrid-institute.com

Acknowledgements

This work was supported by a grant overseen by the French National Research Agency (ANR) as part of the "Investissements d'Avenir" Program ANE-ITE-002-01.

Keywords

≪MMC≫, ≪IGCT≫, ≪Fast recovery diode≫, ≪Failure modes≫, ≪Reverse recovery≫

Abstract

IGCTs are attractive power semiconductor devices for HVDC applications. However, their switching speed at turn-on can only be controlled by the means of an external snubber circuit, which adds complexity and cost. This paper investigates experimentally the possibility to downsize and even completely remove this turn-on snubber/clamp in the case of an MMC submodule based on 6.5 kV IGCTs, using fast silicon diode modules (rated at up to 13 kA µs^{-1}). The removal is found to be possible, although limiting phenomena (dynamic avalanche and snap-off) appear, reducing the actual operating range of the submodule.

1 Introduction – Relevance of IGCTs for HVDC MMCs, turn-on snubber

1.1 The Modular Multilevel Converters and the IGCT

The Modular Multilevel Converter (MMC) is a Voltage Source Converter (VSC) used for Medium or High Voltage Direct Current (MVDC or HVDC) applications. The MMC (Fig. 1a) is based on submodules (SMs), its elementary building blocks. Composed mainly of switches and a capacitor, a submodule can be seen as a small voltage source that can be inserted or not. The half-bridge submodule (HB, shown in Fig. 1b) is the most common submodule type. It consists of two switches and their freewheeling diode, one capacitor (and auxiliary systems, not shown here).

Most submodule designs, such as those described in [1], use IGBTs as controlled switches. These transistors offer high ratings (up to 6.5 kV and a few kA for commercially available IGBTs); their control circuitry is simple and requires low power. However, IGCTs are increasingly considered a potential competitor for IGBTs in HVDC MMCs, and several papers have shown that IGCTs may be a better alternative [2, 3, 4, 5, 6]. Indeed, they have the following advantages: lower losses (studied notably in [2, 3, 4, 5]) as well as higher power ratings than the IGBTs [5]. They also have a short-circuit failure mode, which is very desirable in HVDC MMCs as it permanently bypasses a failed submodule. IGCTs also exhibit some drawbacks, which may explain that the device was not considered for HVDC MMC submodules at first. Perhaps the main drawback is the need for a "turn-on snubber", described below.

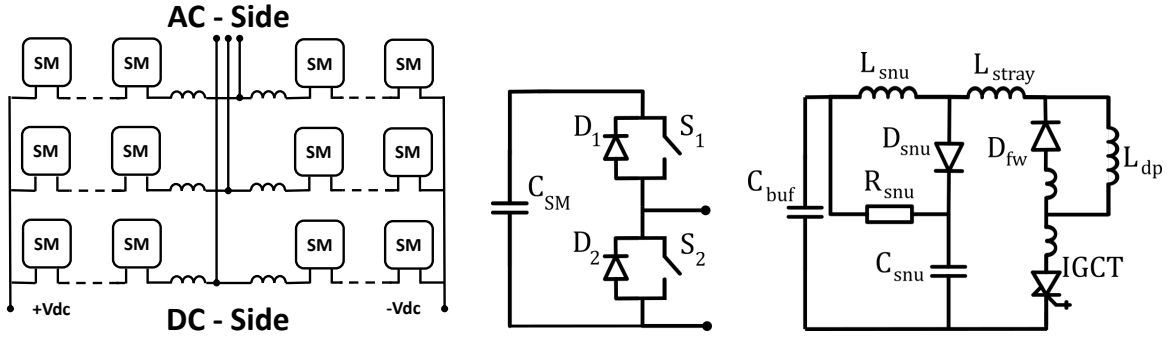

(a) Typical MMC.

(b) Simplified Half-Bridge (HB) SM.

(c) Double test circuit diagram of this paper, submodule part, with a snubber.

Fig. 1: Typical MMC and submodule, and the submodule double pulse circuit used for the tests in this paper.

1.2 Turn-on snubber requirement for IGCT MMC submodules

Based on a thyristor structure, IGCTs do not offer a way to control the speed of their turn-on transient, and in particular, the current slope (di/dt). This turn-on transient can be very fast (tens of kA µs^{-1}), and can cause an excessive burden on the opposite antiparallel diode [2, 3, 6, 7, 8, 9], which can be destroyed as shown in [6] and later in this paper. Indeed, typical silicon power diodes can only sustain di/dt of one or a few kA µs^{-1} at turn-off (which corresponds to the opposite IGCT turning on). At a high di/dt, a diode faces the risk of destruction by dynamic avalanche. According to [10, 11], a high di/dt provokes a high peak power inside the diode at the end of the reverse recovery (when the diode voltage rises), with an indicative 'silicon limit' of 250kW/cm². Consequently, the current slope must be limited externally using a "turn-on snubber" circuit (presented in the figure 1c). The turn-on snubber comprises a snubber inductor (L_{snu} to set $di/dt = V_{bus}/L_{snu}$) and an RCD-clamp (resistor R_{snu}, capacitor C_{snu} and diode D_{snu}, to clamp the overvoltage produced by the snubber inductor at turn-off). The inductor is designed to limit turn-on speed to a value of around 1 kA µs^{-1}, consistent with the recommended diodes (the 5SDF20L4520 from Hitachi, intended for use in IGCT converters, is rated at 1.2 kA µs^{-1}).

It should be noted that the turn-on snubber has the advantage of improving the internal short-circuit capability of the submodule [12, 13, 14]: indeed, if both IGCTs of a SM happens to be ON simultaneously, the SM capacitor is short-circuited; the short-circuit current is then limited by the presence of the snubber inductor. This situation can occur with an erroneous triggering of the initially open IGCT (while the other IGCT is still on) or a failure to turn off an IGCT before turning-on the other. In [12], the snubber inductor is estimated to result in 5 to 10 times short-circuit current peak reduction compared to an IGBT-based SM, which does not contain such snubber.

However, this snubber represents added volume, added cost (4 more parts, including a high voltage diode, D_{snu}) and added switching losses (8 J for a 4 µH snubber inductor and 2 kA SM current for example). Consequently, it may be interesting to downsize it as much as possible. This is for example studied in [2, 6] for 2.2 kV/1.5 kA submodules using press-pack diodes. In these studies, the typical µH-range snubber inductor is reduced down to 320 nH, with the RCD-clamp remaining un-touched. A snubber inductor of 320 nH is comparable to the stray inductance encountered in standard IGCT circuits (L_{stray} in the figure 1c). These studies also demonstrate that the IGCTs themselves can withstand di/dt values higher than the recommended limit of 1 kA µs^{-1} (according to the IGCT datasheet), which suggests that the main limitation to increasing the turn-on speed is the capability of the corresponding diode.

1.3 Aim of the study

In this paper, we investigate the possibility of removing entirely the snubber (smallest possible inductance and no RCD-clamp) in IGCT-based MMC submodules, or at least downsizing even further, compared with the studies in [2, 6], providing that fast enough freewheeling diodes are used. This dramatic simplification of the power circuit would have significant consequences on the cost and volume of an MMC submodule. It is studied experimentally with very fast silicon diodes (up to 13 kA µs^{-1}).

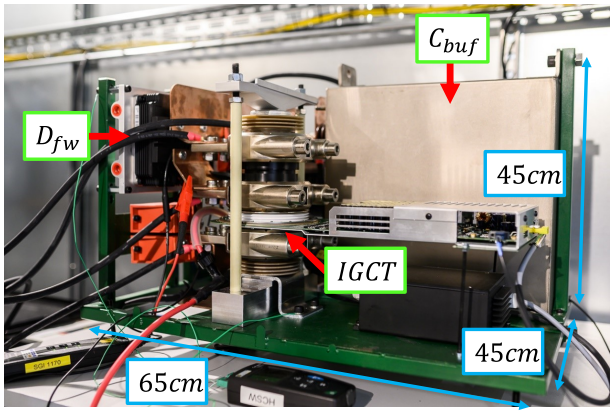

(a) IGCT side of the actual experimental setup.

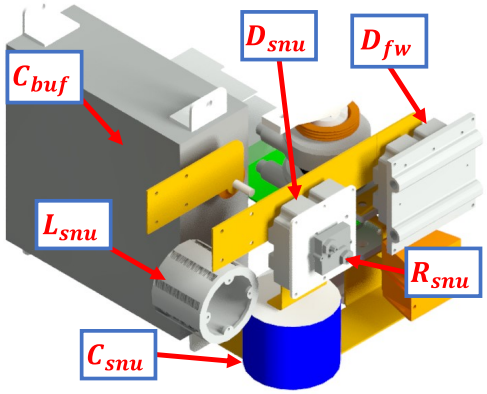

(b) Snubber side, with the cable inductor as the snubber inductor, 3D rendering (AutoCAD).

Fig. 2: The experimental setup used for commutation tests (double pulse).

Table I: Overview of the different parts of the setup with their corresponding ratings, technologies, and part number (if applicable).

Part	Value/Ratings	Technology	Model
L_{snu}	0.8 to 3.4 µH, and 100 to 160 nH	- Air inductor (3D printed mandrel, Figs. 4a 4b) - Busbar connections (Figs. 4c 4d)	Custom
R_{snu}	0.5 Ω	Planar resistor	TAP800KR50E (Ohmite)
C_{snu}	5 µF/6 kV	Film capacitor	E51.S11-502R20 (UPE)
D_{snu}	6.5 kV/2×600 A	6.5 kV Si Diode	5SLD 0600J650100 (Hitachi)
C_{buf}	0.8 mF/3.8 kV	Film capacitor	Trafim (AVX)
L_{dp}	0.4 to 2.8 mH	Air inductor	Custom
L_{stray}	450 nH	*Non applicable*	*Non applicable*

In the next section, the design of the test bench is presented, with the selection of the semiconductors devices and the design of a configurable turn-on snubber. Then (in section 3), the results of the experiment are described and analysed for a reduced snubber inductance as well as for complete removal of the snubber circuit; finally, a particular focus is given to the limiting phenomena that appeared during the experiment, and their associated destructive events.

2 Design and characteristics of the test setup

To analyse the commutations of the IGCT, a ”double-pulse test” circuit is used here. The experimental setup reproduces the possible layout of an HVDC MMC Half-Bridge submodule (although only one IGCT is mounted for the tests presented here) and shows similar behaviour. Therefore, conclusions can be extrapolated to the case of a real HVDC MMC submodule. The experimental setup is shown in figures 2a (IGCT side) and 2b (snubber side). The ratings and technologies of the components used for the test bench can be found in Tab. I (except for the IGCT and diodes, discussed further below). As a reminder, the test setup, with the corresponding components labels, is displayed in figure 1c. The temperature of the semiconductors is controlled by the radiator placed behind the diode pack and the heatsinks of the IGCT pressing clamp. They are connected to a Julabo A40 (thermostat) with EPDM Rubber pipes using HL60 cooling liquid to reach temperatures up to 120 °C.

2.1 Selection of power semiconductors devices

Various IGCT component references available on the market have been listed, without considering RC-IGCTs (as the diode they include is not rated for high di/dt). The list can be found in [15]. Here, we select a 6.5 kV device, as it allows higher voltage operation, a general trend in MMCs, and allow

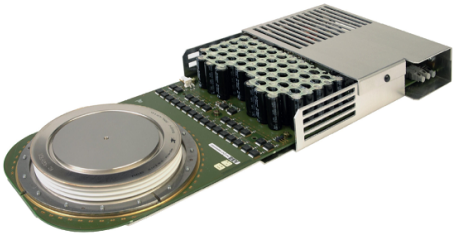

(a) IGCT 5SHY42L6500

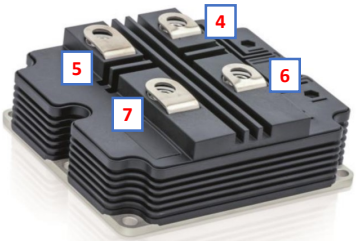

(b) Diode packs (same package for both models).

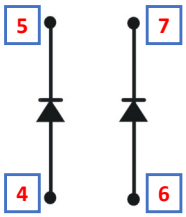

(c) Diode electric connections.

Fig. 3: Photograph of the selected semiconductor devices.

Table II: Noticeable parameter values for the study. 3.6 kV corresponds to a typical bus voltage for a 6.5 kV device (55 % de-rating to ensure 100 FIT reliability). 2.8 kV corresponds to a typical bus voltage for a 4.5 kV device.

Conditions	**di/dt Value**	**Voltage**	**Snubber inductor**
Recommended di/dt for IGCT (w/ 6.5 kV diode)	1 kA µs^{-1}	3.6 kV	3.6 µH
Maximum di/dt (2×diode 6.5 kV)	8 kA µs^{-1}	3.6 kV	450 nH
Recommended di/dt for IGCT (w/ 4.5 kV diode)	1 kA µs^{-1}	2.8 kV	2.8 µH
Maximum di/dt (2×diode 4.5 kV)	13 kA µs^{-1}	2.8 kV	215 nH

testing of both 4.5 and 6.5 kV diodes. The selected IGCT is the 5SHY42L6500 from Hitachi, rated at 6.5 kV/3.8 kA). The current capability of this device is fully compatible with typical HVDC MMCs [5].

Regarding the selection of the freewheeling diode, the main criterion is its maximum allowed di/dt during turn-off, regardless of its package. Indeed, press-pack diodes are typically used together with IGCTs, which are all press pack devices, but most fast diodes, which are intended to be used with IGBTs, tend to be packaged in plastic module cases. For the sake of the study, all suitable diodes are investigated, and some diode modules are found to be the most promising devices: The 5SLD0600J650100 (6.5 kV, 2×600 A, 2×4 kA µs^{-1}) and 5SLD1200J450300 (4.5 kV, 2×1200 A, 2×6.5 kA µs^{-1}). In figure 3b, the diode package used here is displayed (both diodes have the same package). It contains two separate sets of diode chips, as shown in figure 3c. In this study, these two separate diodes are connected in parallel to double the current rating and di/dt. Note that for the sake of simplicity in the setup, the diode used in the RCD-clamp is one 5SLD0600J650100, although its current rating is much larger than required.

2.2 Snubber design

Suitable snubber inductance values depend on bus voltage (V_{bus}) and desired di/dt according to $L_{snu} = V_{bus}/(di/dt)$. Snubber inductor allowing to reach noticeable di/dt values recommended are displayed in Tab. II for the maximum voltage considered ($V_{bus} = 3.6$ kV for 6.5 kV devices and $V_{bus} = 2.8$ kV for 4.5 kV devices).

Custom snubber inductors ranging from 0.8 to 3.4 µH are formed by winding a cable around a 3D-printed mandrel, as shown in figures 4a and 4b. The different values are obtained by printing mandrels with different numbers of turns (2 turns for 800 nH, 3 for 1350 nH, etc.). The space between each turn ensures suitable clearance and creepage distance (low voltage cable is used so that insulation is ensured by the proper spacing). For lower inductance values, we take advantage of the stray inductance of the busbars as it is done in [2, 6], resulting in snubber inductance values of 160 and 100 nH (Figs. 4c and 4d, respectively). An extra stray inductance, evaluated at 450 nH by ANSYS Q3D finite elements calculations, must be added to all these values to obtain the total loop inductance. It corresponds to the unclamped stray inductance of the yellow parts in Fig. 2b.

The capacitor and resistor are selected after iterative circuit simulations using LTSpice, with two criteria: allowing pulses as short as the 40 µs (the minimum pulse time of the IGCT, as quoted in its datasheet) and the tolerated overvoltage on the commutation cell. Their ratings can be found in table I. More details

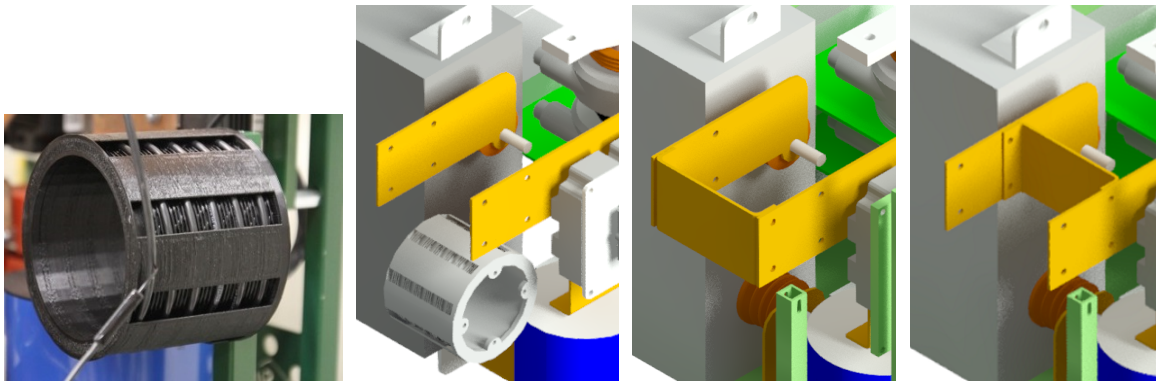

(a) (b) (c) (d)

Fig. 4: Snubber inductor: technical choices to obtain different values from 100 nH to 3.4 µH.

on the selection process can be found in [15].

Although the snubber is not particularly optimised in size here (and no thermal analysis has been performed to allow continuous operation), its volume for this test setup is between 15L to 20L (calculated with AutoCad). This gives a good idea of typical volumes occupied by snubbers and confirms that this volume is significant. The entire snubber can be seen in Fig. 2b.

3 Experimental plan and results

3.1 Experimental plan

A "double pulse" test setup is used to explore a large range of switching current/voltage values, with moderate power dissipation (and therefore limited self-heating). In Fig. 1c the power circuit of the test setup is displayed and in [15] the whole circuit is detailed along with more explanations on the "double pulse". In the results presented below, we focus on the waveforms at the IGCT's turn-on, i.e. when the snubber circuit controls the current transient. The analysed physical quantities are the different reverse recovery parameters of the diode (E_{rr}, T_{rr}, Q_{rr}, I_{rr}), di/dt, the maximum voltage across the diode (and associated overvoltage), the total energy during turn-on ($E_{rr}+E_{on-IGCT}+E_{L-snubber}$) and the peak power during reverse recovery. The measurements are performed for the following conditions:

- Temperature: 25 °C, 60 °C, 90 °C, 120 °C for the heatsinks temperature.
- Voltage: 800 V, 1100 V, 1400 V, 1700 V, 2000 V, 2400 V, 2800 V, 3300 V*, 3600 V*. (* = 6.5 kV diode only)
- Current: 100 A, 300 A, 600 A, 900 A, 1200 A, 1800 A, 2400 A.
- The two diode modules described in section 2.1: the 6.5 kV PM diode and the 4.5 kV PM diode.
- Snubber inductor: 3.42 µH, 2.9 µH, 1.97 µH, 1.34 µH, 0.8 µH (wound inductors, see Fig. 4a), 160 nH, 100 nH (busbar connections). An unclamped stray inductance of 450 nH has to be added to the snubber inductance to obtain the total loop inductance of the circuit.

Due to undesirable phenomena (such as snap-off or dynamic avalanche), not all configurations of the parameters above are possible. This is especially true for the 6.5 kV diode, for which some failures are observed (this is described further below).

3.2 Typical waveforms and occurrence of snap-off

In this subsection, typical waveforms are presented at IGCT turn-on (see figure 5). Two types of reverse recovery can be observed: soft-recovery (figure 5a, in which the diode current – I_{FWD} – smoothly reaches zero after recovery) and snappy-recovery (figure 5b, for which the diode current abruptly returns to zero at the end of the reverse recovery, causing oscillations). The chronology for the soft recovery (figure 5a) is the following:

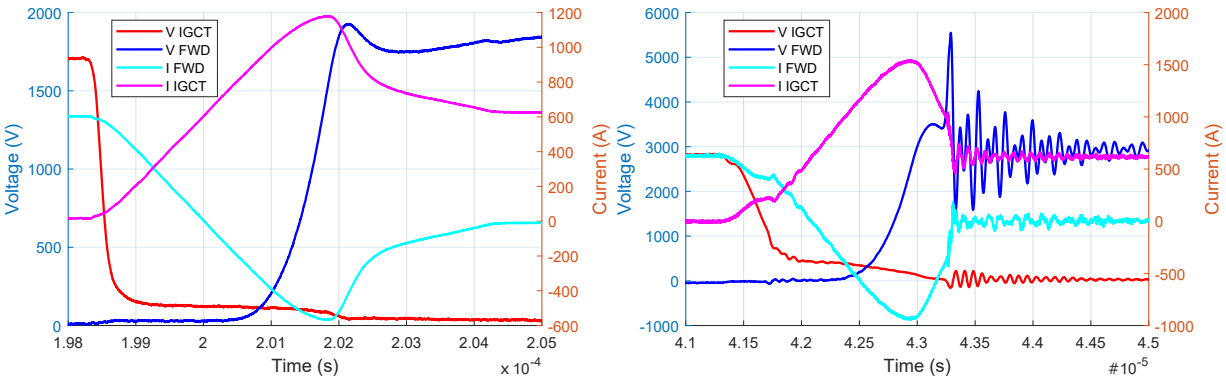

(a) Soft reverse recovery.

(b) Snappy reverse recovery.

Fig. 5: Typical waveforms obtained during the measures. Left: pulse at 1700 V/600 A/120 °C with the 4.5 kV diode and a 3.4 µH snubber inductor. Right: pulse at 2800 V/600 A/25 °C with the 6.5 kV diode and a 2.9 µH snubber inductor.

1. The IGCT receives the turn-on command and its voltage (V_{IGCT}, in red) starts decreasing ($t = 198.2\,\mu s$). The diode current (I_{FWD}, cyan) starts to transfer to the IGCT (I_{IGCT}, pink). This first phase ends when the IGCT voltage has finished its first decrease and is stable at a low voltage ($t = 199\,\mu s$).
2. Then, the current still transfers from the diode to the IGCT at a constant rate, determined by the loop inductance value; this loop inductor sustains most of the bus voltage during this phase. This second phase ends when the diode starts blocking voltage ($t = 200.5\,\mu s$).
3. The voltage across the diode (V_{FWD}, blue) increases as the diode enters reverse recovery. The reverse recovery current reaches its minimum (I_{rr}) at $t = 201.9\,\mu s$.
4. Starting from $t = 202.2\,\mu s$, a smooth recovery takes place: dI_{FWD}/dt slowly decreases until the recovery is over ($t = 204.3\,\mu s$).

In some cases, diodes can also display a "snappy recovery" behaviour, such as depicted in figure 5b. The abrupt diode current slope at $t = 43.2\,\mu s$ generates an overvoltage spike and oscillations that can be destructive [11, 16, 17]. Diode manufacturers optimise their devices to avoid snappy behaviour (among other criteria), adjusting doping levels and lifetime profile in the semiconductor [16], but, as described in [18], even soft diodes can present a snappy behaviour in certain conditions. In [16], operational conditions that favour snap-off are listed: low temperature, high voltage, high stray inductance, and low current.

3.3 Main results

This section starts with two subsections investigating the main stresses experienced by the diode (peak power density, overvoltage) and their evolution with current, voltage, L_{snu}, di/dt, temperature, and presence (or not) of an RCD clamp. Then, we analyse the impact of the snubber reduction and removal on the losses during turn-on. Finally, we focus on the impact of removing the RCD-clamp altogether.

In summary, it is possible to reduce the snubber inductance down to its lowest possible value (100 nH) for the 4.5 kV diode and even remove the RCD-clamp: proper operation is observed up to 2.4 kV and 1.8 kA at a temperature of 90 °C and 120 °C (up to 1.7 kV 2.4 kA for 25 °C and 60 °C). The 6.5 kV diode is found to work for a 800 nH inductor up to 3.6 kV/2.4 kA, but to fail at a lower snubber inductor (160 nH), as described in section 4.2.

3.3.1 Maximum power during reverse recovery

The maximum power densities measured for the 4.5 kV diode during reverse recovery are plotted in Fig. 6 over the voltage, current domain, for different snubber inductor values. This maximum power is calculated as the maximum of the $I_{FWD} \times V_{FWD}$ product divided by the total diode surface inside a package (active surface per die times the number of dies) assumed to be 19.44 cm^2 for the 4.5 kV diode

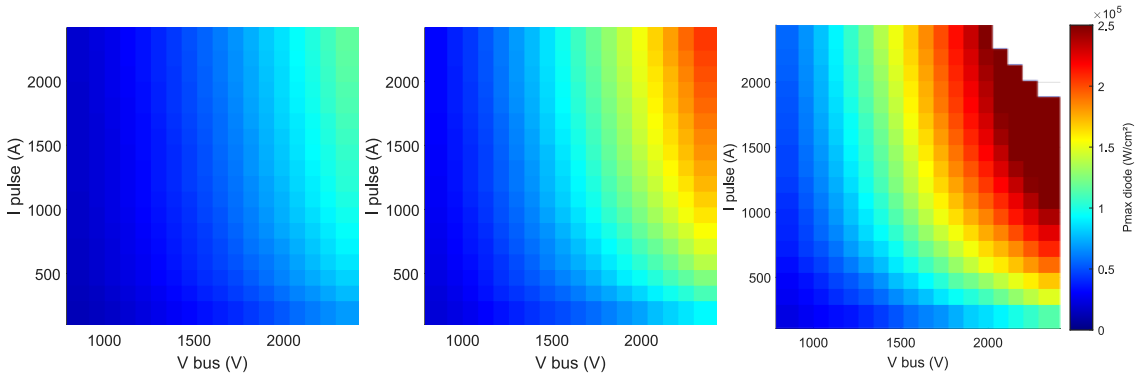

(a) 3.42 µH (b) 0.8 µH (c) 100 nH + no RCD-clamp.

Fig. 6: Maximum power density (W/cm²) in the 4.5 kV diode during reverse recovery, depending on the snubber inductor and structure, at 120 °C. The scale's maximum is the indicative 'silicon limit': 250kW/cm².

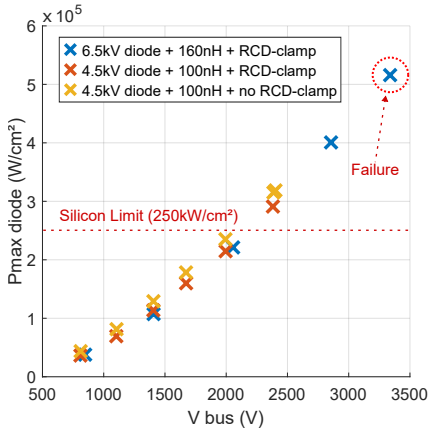

Fig. 7: Maximum power density (W/cm²) in the two diodes during the reverse recovery. In blue, for the 6.5 kV diode, 25 °C, 2400 A, 160 nH snubber inductance and RCD-clamp. In yellow and orange, for the 4.5 kV diode, 120 °C, 1800 A, 100 nH snubber inductance. In orange: RCD-clamp present, in yellow: RCD-clamp absent.

and 19.44 cm^2 as well for the 6.5 kV diode.

It can be seen that reducing the snubber inductance (and therefore increasing the di/dt at the IGCT turn-on) increases the peak power dissipation of the diode. In figure 6c, the indicative threshold of the "silicon limit" (250 kW cm^{-2}), described in [10], is even exceeded, but it did not lead to destruction. Fig. 7 presents the peak power density as a function of the bus voltage, for the most critical situations (i.e., lowest tested L_{snu}). The 6.5 kV diode is found to fail at a power level of 516 kW cm^{-2}, after a successful test at 401 kW cm^{-2}. This is in the order of magnitude of the indicative "silicon limit" [10, 11].

These results confirm that downsizing the snubber leads to higher stress on the diode during the reverse recovery, but they also demonstrate the possibility to minimise the snubber inductance value and to remove the RCD-clamp over a significant part of the (voltage,current) domain without causing diode failure.

3.3.2 Overvoltage across the diode due to snappy-recovery

As shown in Fig. 5b, the snap-off phenomenon causes a large overvoltage to appear across the diode (V_{FWD}) at the end of its recovery. This overvoltage spike may cause avalanche in the diode if it exceeds its blocking capability and eventually leads to the destruction of the device.

Fig. 8 presents the amplitude of the overvoltage (i.e. the difference between the overvoltage peak and the bus voltage). The overvoltage scale in the figure is blocked between 500V (when an overvoltage starts to be significant) and 1000V (when an overvoltage is too severe) in order to emphasise the phenomenon do-

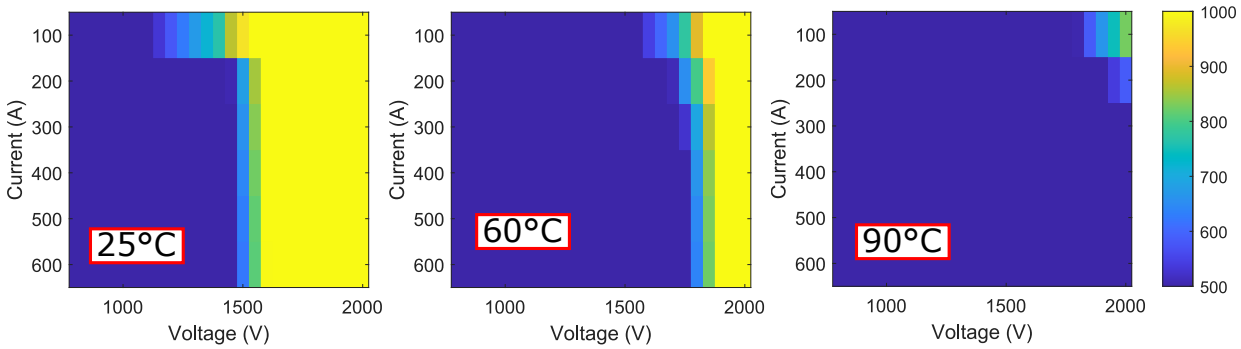

(a) Ambient temp. (25 °C). (b) 60 °C. (c) 90 °C.

Fig. 8: Heatmaps representing the overvoltage level depending on voltage, current, and temperature during snap-off events. Diode used here: 4.5 kV diode. L_{snu}=3.4 µH.

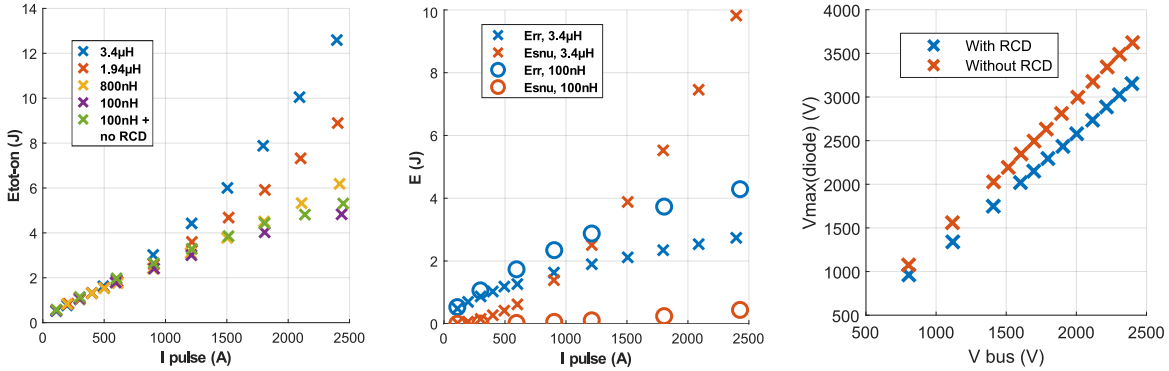

(a) Total turn-on losses for various snubber inductors. 2 kV, 120 °C.

(b) Turn-on losses break-down for two snubber inductors. 2 kV, 120 °C.

(c) Max. Voltage for the cases with or without RCD clamp. 600 A, 120 °C.

Fig. 9: Different results of the double pulse test (turn-on losses, maximum voltage).

main. It shows that, in the case presented here, significant snap-off occurs, with overvoltages exceeding 1000 V over a large fraction of the (I,V) domain, especially for the lowest junction temperature.

The trends are consistent with the literature [16]: diode snap-off is reported to depend on temperature, voltage, current, and stray inductance. Higher voltage, lower current, or/and lower temperature increase the snap-off overvoltage. In [15, 19], the effect of stray inductance on snap-off behaviour has been demonstrated. Here, the relatively high value of the stray inductance of our test setup (450 nH, in addition to the clamped snubber inductor) is suspected to be the reason why the snap-off occurs at these levels of voltage/current/temperature (as a comparison, datasheet values are quoted for a stray inductance value of 150 nH for the 4.5 kV diode). Reducing the stray inductance of the test setup is therefore required to reduce the area of the operational domain where snap-off occurs.

3.3.3 Snubber reduction impact on losses

The total switching energy losses ($E_{rr} + E_{on-IGCT} + E_{L-snubber}$) during IGCT turn-on are displayed in Fig. 9a, for 2 kV, 120 °C and various snubber inductors. This graph shows a clear reduction of the switching losses, especially for the highest current values, as the snubber inductor is reduced from 3.4 µH down to 100 nH.

Figure 9b explains this phenomenon, with the 3.4 µH snubber inductor situation marked with a cross ('x') and the 100 nH snubber inductor situation indicated with a circle ('o'): indeed, while the reverse recovery energy (in blue) is $\approx 50\,\%$ higher for the 100 nH snubber inductor than for the 3.4 µH, the energy dissipated by the snubber inductor (in orange) is drastically reduced (in the order of a 20-fold reduction). Downsizing the snubber inductor therefore offers a clear advantage regarding turn-on losses.

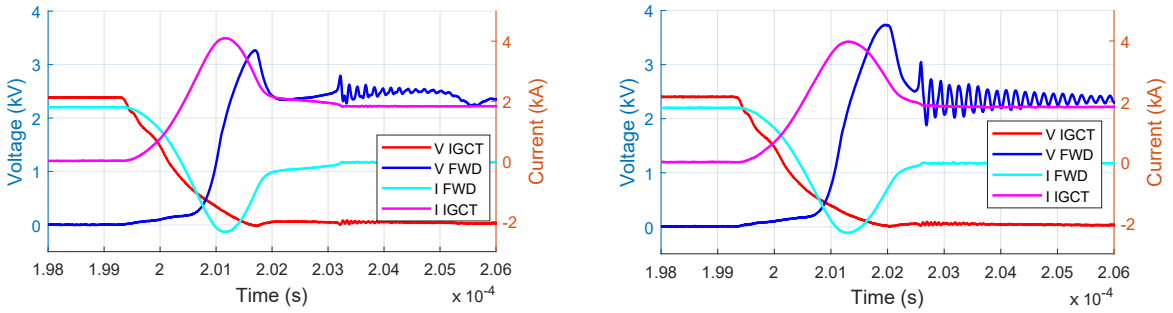

(a) With RCD.

(b) Without RCD.

Fig. 10: Waveforms of cases with and without RCD clamp. 2400 V, 1800 A, 120 °C, 4.5 kV diode, L_{snu}=100 nH.

3.3.4 Operation without snubber

Tests without RCD clamp (in the case of the 100 nH inductor) are completed up to 2.4 kV and 1.8 kA at 120 °C and 90 °C, and 1.7 kV and 600 A at 25 °C with the 4.5 kV diode.

Waveforms of tests with and without RCD clamp are displayed in Fig. 10. The resulting peak voltages are depicted in Fig. 9c at 120 °C and 600 A. Removing the RCD Clamp only results in a moderate increase of the turn-on losses (green and purple markers in Fig. 9a). This is confirmed in Fig. 9c, which shows that the peak voltage experienced by the diode increases by $\approx 15\,\%$. It is comparable with the increase in loop inductance: 450 nH in the clamped case (stray inductance only), $450 + 100$ nH in the un-clamped case (stray inductance + snubber inductor), i.e. a 22 % increase.

As shown in Fig. 9a, losses without RCD (green) are therefore increased compared to the case with RCD (purple) but are still lower than the losses with a 0.8 µH inductor (and RCD clamp). It must be noted that the increase in loop inductance caused by removing the RCD-clamp results in a slightly higher maximum power density inside the diode for the same voltage and current, as shown in Fig. 7 (at 2.4 kV/1.8kA/120 °C: 290 kW cm^{-2} with RCD, 315 kW cm^{-2} without RCD).

4 Limiting phenomena and failure events

Two destructive events are encountered during the tests. One is directly related to the snap-off of the diode, the other to dynamic avalanche. These two failure events are displayed in Fig. 11 and are explained in this section.

4.1 Snap-off

Snap-off can be destructive, as the resulting overvoltage can exceed the blocking capability of the diode. This is the case in the waveforms in Fig. 11a, for which a peak voltage of 5.8 kV is observed across the 4.5 kV diode. Analysis of the failed device shows that 3 of the diode chips in the diode package show clear signs of degradation (Fig. 11c), with ”trenches” at the surface which are indicative of a focused phenomenon (filamentation, which causes localised melting of the silicon). More details about this failure mechanism can be found in [11, 15, 16, 17].

4.2 Dynamic avalanche

The dynamic avalanche occurs at a lower voltage than the static breakdown voltage of the diode, during reverse recovery. During turn-off, the diode blocks an increasing voltage, which is supported by the depletion region that grows within the drift region. But in certain conditions, especially at high di/dt, the electric field at the PN junction reaches a value higher than the limit (35 kV mm^{-1}), leading to the destruction of the device. The destructive dynamic avalanche (also called 3rd-degree dynamic avalanche) is described in more detail in [11, 15, 16, 20].

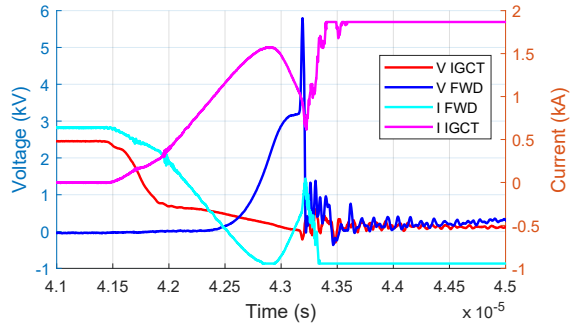

(a) Waveforms of failure event due to snap-off.

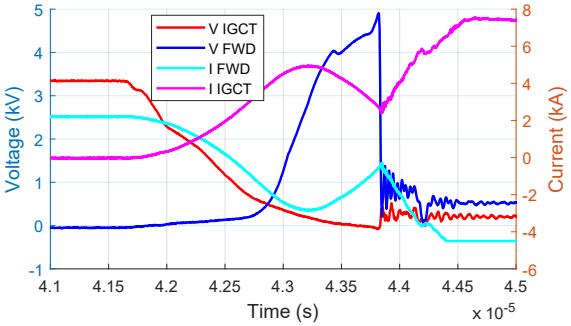

(b) Waveforms of failure event due to dynamic avalanche.

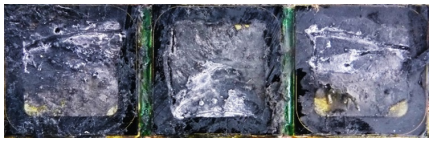

(c) Dies after snap-off destruction.

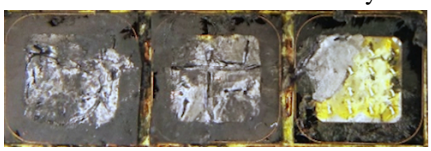

(d) Dies after dynamic avalanche destruction.

Fig. 11: Failure events during tests. (a-c-e) Snap-off destructive event: 2400 V, 600 A, di/dt of 1.7 kA µs^{-1}, 25 °C. Used diode for the pulse: the 4.5 kV. (b-d-f) Dynamic avalanche destructive event: 3300 V, 2200 A, di/dt of 4.5 kA µs^{-1}, 25 °C. Used diode for the pulse: the 6.5 kV.

Fig. 11b shows the waveforms of a failure event attributed to dynamic avalanche, for the 6.5 kV diode. Compared with the snap-off case (Fig. 11a), V_{FWD} does not exhibit a sharp peak and does not exceed the static blocking voltage of the diode. dI_{FWD}/dt, is relatively high, at 4.5 kA µs^{-1} (the diode module, which contains two separate groups of diode chips is rated at 2×4 kA µs^{-1}), and the test current is twice that of the package (2400 A vs. 2×600 A). This, together with the relatively large stray inductance (450 nH compared to 280 nH considered for the datasheet SOA figures) led to the diode failure.

Conclusion

Reducing the snubber inductor or removing the RCD clamp in an IGCT-based MMC submodule is found to be possible without failure at levels up to 2.4 kV/1.8 kA (using the 4.5 kV diode). A smaller snubber leads to lower losses and overall volume (15 L reduction). Removing the RCD clamp slightly increases switching losses, but the total losses (semiconductor devices and snubber circuit) remain lower than those observed in the standard case of 3.4 µH inductor and an RCD clamp (5.5 J and 13.5 J respectively, at 2 kV/2.4 kA/120 °C).

Limiting phenomena are observed (snap-off and dynamic avalanche). In real HVDC MMC implementations, they would be important problems as they occur within the normal operating range of the converter. Indeed, the observed overvoltage at ambient temperature is higher than 1 kV at 1700 V for the 4.5 kV diode. The relatively high stray inductance of the circuit could be significantly reduced in order to: (i) reduce the overvoltage during commutations and therefore the losses, (ii) reduce the occurrence and intensity of the snap-off, (iii) reduce the constraints due to high di/dt and reduce the risk of dynamic avalanche. It is estimated that re-arranging the various components of the system could yield a reduced loop inductance of less than 250 nH. Another solution to overcome these issues would be to use silicon carbide diodes, which have lower reverse recovery (or no reverse recovery at all in the case of Schottky diodes). The higher cost of these devices could be offset by the removal of the snubber circuit, the gains in efficiency and the simpler design of the structure.

References

[1] Kamran Sharifabadi, Lennart Harnefors, Hans-Peter Nee, Steffan Norrga, and Remus Teodorescu. *Design, Control, and Application of Modular Multilevel Converters for HVDC Transmission Systems*. John Wiley & Sons Inc, 2016.

[2] Rong Zeng, Biao Zhao, Tianyu Wei, Chaoqun Xu, Zhengyu Chen, Jiapeng Liu, Wenpeng Zhou, Qiang Song, and Zhanqing Yu. Integrated gate commutated thyristor-based modular multilevel converters: A promising solution for high-voltage dc applications. *IEEE Industrial Electronics Magazine*, 13(2):4–16, jun 2019.

[3] Davin Guédon, Philippe Ladoux, Mehdi Kanoun, and Sébastien Sanchez. Igcts in hvdc systems: Analysis and assessment of losses. In *PCIM Europe 2019*, 2019.

[4] Tomas Modeer, Hans-Peter Nee, and Staffan Norrga. Loss comparison of different sub-module implementations for modular multilevel converters in HVDC applications. *EPE Journal*, 22(3):32–38, sep 2012.

[5] Arthur Boutry, Cyril Buttay, Dong Dong, Rolando Burgos, Bruno Lefebvre, Florent Morel, and Colin Davidson. Figures-of-merit and current metric for the comparison of igcts and igbts in modular multilevel converters. In *2020 22nd European Conference on Power Electronics and Applications (EPE'20 ECCE Europe)*, pages P.1–P.10, 2020.

[6] Tianyu Wei, Qiang Song, Jianguo Li, Biao Zhao, Zhengyu Chen, and Rong Zeng. Experimental evaluation of IGCT converters with reduced di/dt limiting inductance. In *2018 IEEE Applied Power Electronics Conference and Exposition (APEC)*. IEEE, mar 2018.

[7] ABB. Applying igcts. Technical report, ABB, 2016.

[8] Silverio Alvarez-Hidalgo. *Characterisation of 3.3kV IGCTs for Medium Power Applications*. PhD thesis, ENSEEIHT, 2005.

[9] I. Etxeberria-Otadui, J. San-Sebastian, U. Viscarret, I. Perez de Arenaza, A. Lopez de Heredia, and J. M. Azurmendi. Analysis of IGCT current clamp design for single phase h-bridge converters. In *2008 IEEE Power Electronics Specialists Conference*. IEEE, jun 2008.

[10] Josef Lutz and Martin Domeij. Dynamic avalanche and reliability of high voltage diodes. *Microelectronics Reliability*, 43(4):529–536, apr 2003.

[11] Josef Lutz, Heinrich Schlangenotto, Uwe Scheuermann, and Rik De Doncker. *Semiconductor Power Devices*. Springer Berlin Heidelberg, 2011.

[12] David Weiss, Michail Vasiladiotis, Cosmin Banceanu, Noemi Drack, Bjorn Odegard, and Andrea Grondona. Igct based modular multilevel converter for an ac-ac rail power supply. In *PCIM Europe 2017; International Exhibition and Conference for Power Electronics, Intelligent Motion, Renewable Energy and Energy Management*, pages 1–8, 2017.

[13] Philippe Ladoux, Nicola Serbia, and Eric I. Carroll. On the potential of IGCTs in HVDC. *IEEE Journal of Emerging and Selected Topics in Power Electronics*, 3(3):780–793, sep 2015.

[14] Bjørn Ødegård, David Weiss, Tobias Wikström, and Remo Baumann. Rugged mmc converter cell for high power applications. In *2016 18th European Conference on Power Electronics and Applications (EPE'16 ECCE Europe)*, pages 1–10, 2016.

[15] Arthur Boutry. *Theoretical and experimental evaluation of the Integrated gate-commutated thyristor (IGCT) as a switch for Modular Multi Level Converters (MMC)*. Theses, INSA Lyon, December 2021.

[16] M. T. Rahimo and N. Y. A. Shammas. Freewheeling diode reverse-recovery failure modes in igbt applications. *IEEE Transactions on Industry Applications*, 37(2):661–670, 2001.

[17] Katsumi Nakamura, Fumihito Masuoka, Akito Nishii, Shin ichi Nishizawa, and Akihiko Furukawa. Freewheeling diode technology with low loss and high dynamic ruggedness in high-speed IGBT applications. *IEEE Transactions on Electron Devices*, 66(11):4842–4849, nov 2019.

[18] Peter Losee, Max-Josef Kell, Fabio Carastro, Jorge Mari, Matthias Menzel, Tobias Schuetz, and Thomas Zoels. Soft recovery diodes with snappy behavior. In *2015 17th European Conference on Power Electronics and Applications (EPE'15 ECCE-Europe)*. IEEE, sep 2015.

[19] N.Y.A. Shammas, M.T. Rahimo, and P.T. Hoban. Effects of external operating conditions on the reverse recovery behaviour of fast power diodes. *EPE Journal*, 8(1-2):11–18, jun 1999.

[20] B. Heinze, J. Lutz, H.P Felsl, and HA. Schulze. Ruggedness of high voltage diodes under very hard commutation conditons. In *2007 European Conference on Power Electronics and Applications*. IEEE, 2007.